Journal of ELECTRONIC MATERIALS, Vol. 35, No. 5, 2006 *Regular Issue Paper*

Microstructure and Mechanical Properties Evolution of Intermetallics between Cu and Sn-3.5Ag Solder Doped by Ni-Co Additives

F. GAO,[1,2] T. TAKEMOTO,[1] H. NISHIKAWA,[1] and A. KOMATSU[1]

1.—Joining and Welding Research Institute, Osaka University, Osaka, Japan, 567-0047.
2.—E-mail: gaoflj@jwri.osaka-u.ac.jp

The evolution of intermetallic compounds (IMCs) generated between Sn-3.5Ag solder doped by additive couples (namely, 0.2mass%Co and 0.1mass%Ni) and Cu substrate was characterized. After soldering, the additive couples, Co-Ni, were all detected at the intermetallic region. The microstructure of intermetallic was identified as (Cu, Ni, Co)$_6$Sn$_5$ by electron probe microanalysis (EPMA) and x-ray diffraction (XRD). However, the morphology of (Cu, Ni, Co)$_6$Sn$_5$ was converted to columnar like and was not as dense as the typical scallop-like Cu$_6$Sn$_5$. A duplex structure of (Cu, Ni, Co)$_6$Sn$_5$, namely, two distinct regions bearing different concentrations of Ni and Co, was observed. Much higher Ni and Co concentrations were probed in the outer intermetallic region adjacent to the solder matrix, while lower concentration at the inner region was verified. After aging, the intermetallic (Cu, Ni, Co)$_6$Sn$_5$ tended to be dense, while the growth rate was depressed at the early stage. In addition, the Cu$_3$Sn phase was not detected after aging at 110°C, while it appeared at 130°C and 150°C for 504 h. Using the nanoindentation technique, some mechanical properties of (Cu, Ni, Co)$_6$Sn$_5$ were investigated. The lower hardness and Young's modulus of the outer intermetallic region was revealed. After aging treatment, both the hardness and Young's modulus values were elevated.

Key words: Lead-free solder, additive, nanoindentation, intermetallic compounds (IMCs)

INTRODUCTION

The conventional Sn-Pb solder has been switched to lead-free solder, since the ban of lead will take effect as of July 1, 2006. So far, the Sn-Ag solder and its derivations have been regarded as the promising candidates to replace the Sn-Pb solder due to their superior mechanical properties of strength, creep, and fatigue resistance.[1,2] In order to meet the requirements for different applications, appropriate solders are being extensively sought. The alloying method is a simple and effective way of modifying the properties of solders. Elements such as Co, Ni, Zn, Fe, Al, Cu, Sb, and In were considered.[3–5] In particular, it has been reported that the additive Ni or Co could participate in the interfacial reaction between solder and Cu substrate, which results in the morphology change of intermetallic compounds (IMCs).[4–7]

(Received August 16, 2005; accepted August 22, 2005)

However, a more detailed investigation on the morphology of intermetallic and additive distribution is not sufficient. The addition couple, namely, Ni-Co, is added into Sn3.5Ag solder in the current research. Meanwhile, the additive involvement in the interfacial reaction will definitely result in the variation of IMC mechanical properties. Therefore, the novel nanoindentation methodology is employed herein to explore the responses.

EXPERIMENTAL

The copper substrate sheet (99.99% purity, 25 mm × 25 mm × 0.3 mm) was used to react with Sn3.5Ag and Sn3.5Ag0.2Co0.1Ni solders simultaneously. Before reflow experiments, the copper sheet was chemically processed in 5% HCl solution for 20 sec, and then cleaned further ultrasonically in alcohol. The peak soldering temperature was set at 250°C, and the dwell time was 1 min. After soldering, the

remaining solder was etched away by 13% HNO_3 + H_2O solution to reveal the top-view morphology of IMCs. Some solder joints formed between Sn3.5Ag0.2Co0.1Ni and Cu were subjected to aging at 110°C, 130°C, and 150°C for 504 h, respectively. The observation of IMC morphology was performed by scanning electron microscopy (SEM), and electron probe microanalysis (EPMA) was employed to determine the chemical composition of components and their redistribution by color mapping. The crystal microstructure was measured by x-ray diffraction (XRD), while some primary mechanical properties of IMCs such as hardness and Young's modulus were evaluated by nanoindentation (Micro Materials, Wrexham, United Kingdom).

RESULTS AND DISCUSSION

The IMCs formed between Sn3.5Ag0.2Co0.1Ni and Cu exhibited a higher growth rate during soldering than that of Sn-3.5Ag/Cu, as displayed in Fig. 1. Namely, the thickness of intermetallic for Sn3.5Ag0.2Co0.1Ni solder was elevated. Meanwhile, the morphology of intermetallic was converted to be very flat; however, it was not as dense as that for Sn-3.5Ag solder. In particular, some spaces were occupied by the solder entrapped inside intermetallic, which was consistent to the previous results.[7] A more striking phenomenon was observed from the top-view SEM micrographs of intermetallics, as illustrated in Fig. 2. It was quite clear that the intermetallic grains formed between Sn-Ag-Co-Ni solder and Cu were extremely refined, which indicated that the grain coarsening behavior was depressed dramatically, rather different from that for the Sn-3.5Ag/Cu interfacial reaction. The columnar-type intermetallic for Sn-Ag-Co-Ni/Cu was suggested, compared with the typical scallop-like morphology of Cu_6Sn_5. In addition, the growth direction of intermetallic formed between the Sn-Ag-Co-Ni solder and Cu was irregular or scattered, that is, not perpendicular to the interface as for scallop Cu_6Sn_5. The ripening-depressed grains and the irregular growth direction might be responsible for the nondense morphology, namely, the liquid solder filling in the vacancy among IMC grains.

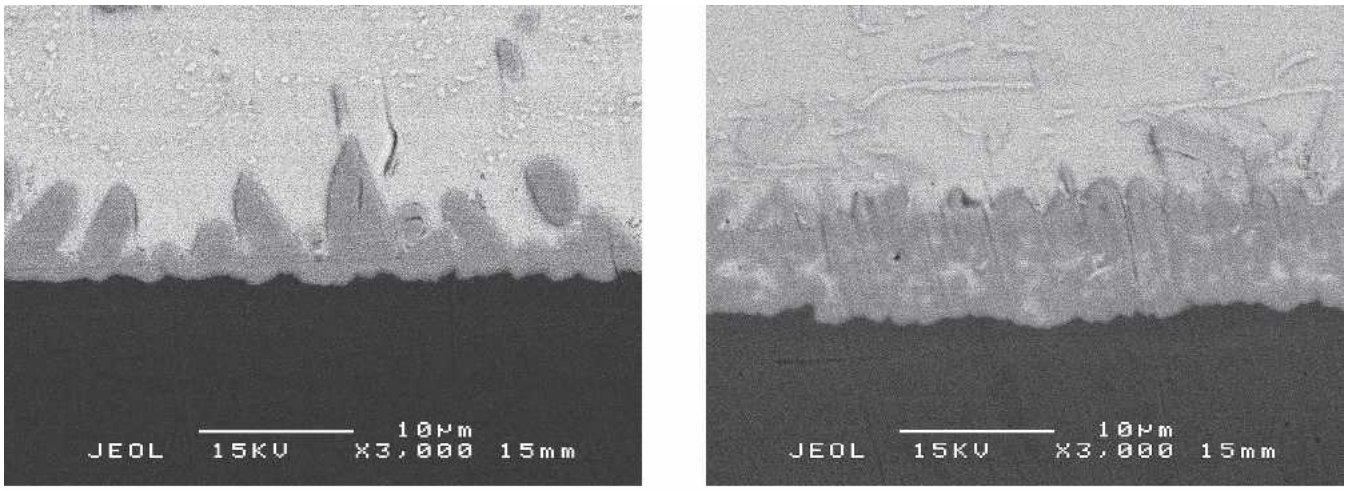

a b

Fig. 1. BEI intermetallic micrograph (cross section) after reflow for 1 min. at 250°C: (a) Sn-3.5Ag/Cu and (b) Sn-3.5Ag-0.2Co-0.1Ni/Cu.

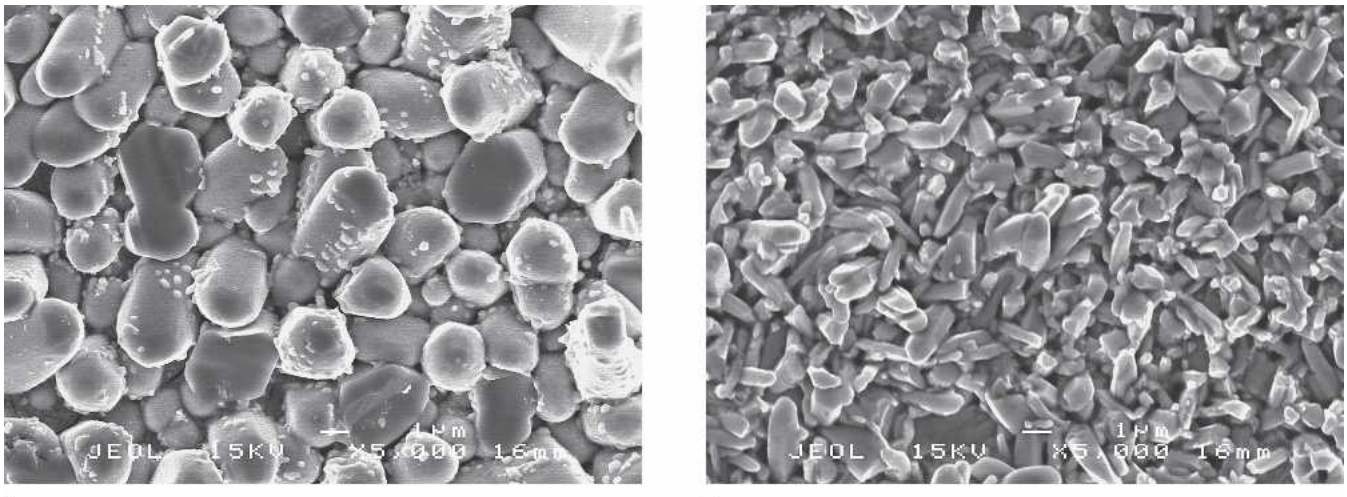

a b

Fig. 2. Comparison of intermetallic morphology (top view), reflow at 250°C for 1 min.: (a) Sn-3.5Ag/Cu and (b) Sn-3.5Ag-0.2Co-0.1Ni/Cu.

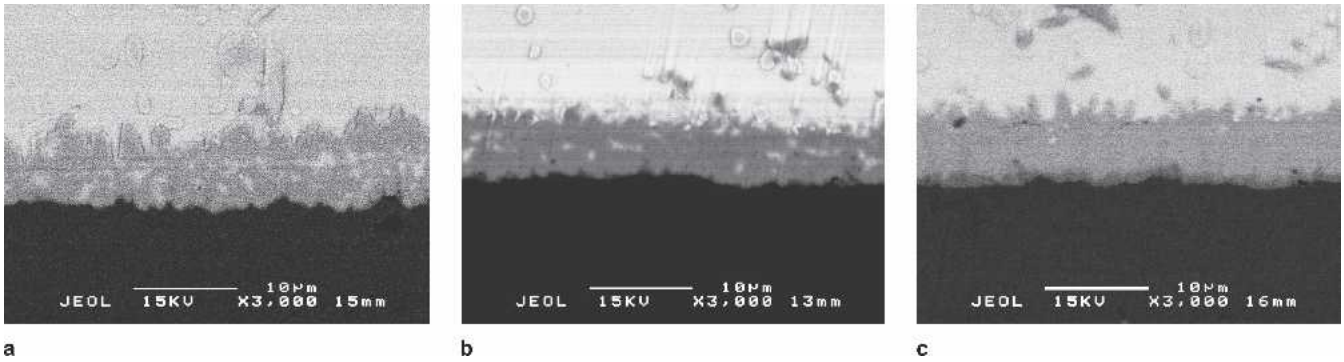

Fig. 3. Comparison of intermetallic morphology (BEI image) of Sn-3.5Ag-0.2Co-0.1Ni/Cu after aging for 504 h at the temperature of (a) 110°C, (b) 130°C, and (c) 150°C.

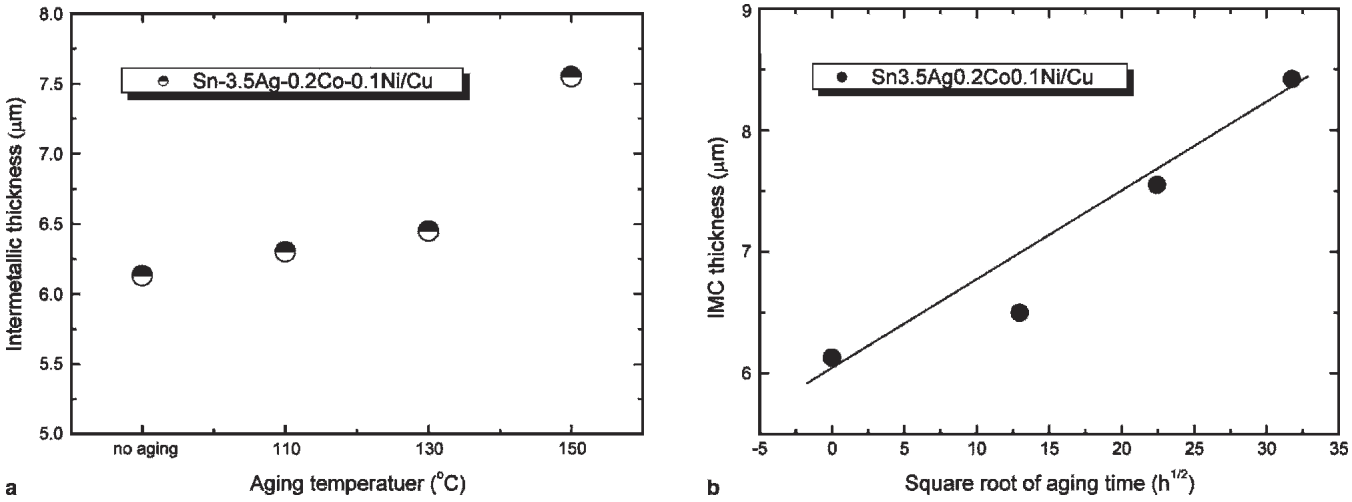

Fig. 4. Intermetallic thickness evolution between Sn-Ag-Co-Ni solder and Cu: (a) after aging at 110°C, 130°C, and 150°C, respectively; and (b) after aging at 150°C for 168 h, 504 h, and 1,008 h, respectively.

Table I. Chemical Compositions of Intermetallic Determined by EPMA

Sn-3.5 Ag-0.2Co-0.1Ni	Sites	Composition (At.%) Sn	Cu	Ni	Co	Phases
No aging	1	46.2	43.3	5.1	5.4	$(Cu_{(1-x-y)}, Co_x, Ni_y)_6Sn_5$
	2	46.3	51.8	1.2	0.7	$(Cu_{(1-m-n)}, Co_m, Ni_n)_6Sn_5$
	3	46.0	53.3	0.5	0.2	
110°C	1	45.7	44.8	4.4	5.1	$(Cu_{(1-x-y)}, Co_x, Ni_y)_6Sn_5$
	2	44.8	53.1	1.4	0.7	$(Cu_{(1-m-n)}, Co_m, Ni_n)_6Sn_5$
	3	45.6	53.8	0.4	0.2	
130°C	1	46.7	46.9	2.5	3.9	$(Cu_{(1-x-y)}, Co_x, Ni_y)_6Sn_5$
	2	47.2	51.6	0.5	0.8	$(Cu_{(1-m-n)}, Co_m, Ni_n)_6Sn_5$
	3	25.5	74.5	—	—	Cu_3Sn
150°C	1	45.7	48.9	1.7	3.7	$(Cu_{(1-x-y)}, Co_x, Ni_y)_6Sn_5$
	2	46.1	52.6	0.4	0.9	$(Cu_{(1-m-n)}, Co_m, Ni_n)_6Sn_5$
	3	25.7	74.3	—	—	Cu_3Sn

After aging at 110°C, 130°C, and 150°C for 504 h, respectively, the intermetallic evolution between Sn-Ag-Co-Ni solder and Cu was presented in Fig. 3. Two results were obtained: (1) the solder entrapped within the intermetallic region tended to be less and (b) the entire thickness of the intermetallic did not increase severely, in particular, at the lower aging temperature. This phenomenon could be interpreted by the Cu atoms diffusion mechanism during the interfacial reaction. Many researchers have suggested that the Cu atoms are the dominant diffusion species for the interfacial reaction between Sn-Ag solder and Cu substrate.[8,9] Thus, the solder entrapped within the intermetallic region reacted with the Cu atoms transported from the substrate. Following the decrease of the solder entrapped in the intermetallic

region, the IMC morphology became dense. In turn, the consumption of Cu atoms during this process reduced the supply flux of Cu atoms for the interfacial reaction that occurred between the solder matrix and intermetallic front line, thus resulting in a relatively slower growth rate of intermetallic during solid aging. Obviously, the higher aging temperature, e.g., 150°C, triggered a faster supply flux of Cu atoms; therefore, the solder entrapped in the intermetallic region was converted into the intermetallic and disappeared. The interface of the intermetallic/solder matrix continued to penetrate into the solder matrix and enhance the growth, as demonstrated in Fig. 4a. In the mean time, as displayed in Fig. 4b, during the early aging time (e.g., 168 h) at 150°C, the growth rate was also relatively depressed, resulting in a shift below the proportional fitting line given by the typical diffusion-control equation $d = d_0 + 2k\sqrt{Dt}$. This indicated that the consumption of entrapped solder could influence the growth rate of IMC during aging, particularly at the early stage.

The Cu_3Sn phase was not generated after aging at 110°C, while it appeared at 130°C and 150°C, as displayed in Fig. 3. For the case aging at 130°C, the Cu_3Sn phase was discontinuously distributed at selected sites along the interface between the primary IMC phase and Cu substrate. At higher aging temperature, say, 150°C, a continuous Cu_3Sn layer with 2–3 μm thickness was observed. These results indicated that the critical temperature for the Cu_3Sn phase generation during aging was between 110°C and 130°C.

The chemical composition of intermetallic was determined by EPMA. Three sites, say, sites 1, 2, and 3, were selected to measure the element contents, as shown in Fig. 3. Site 1 was located in the upper

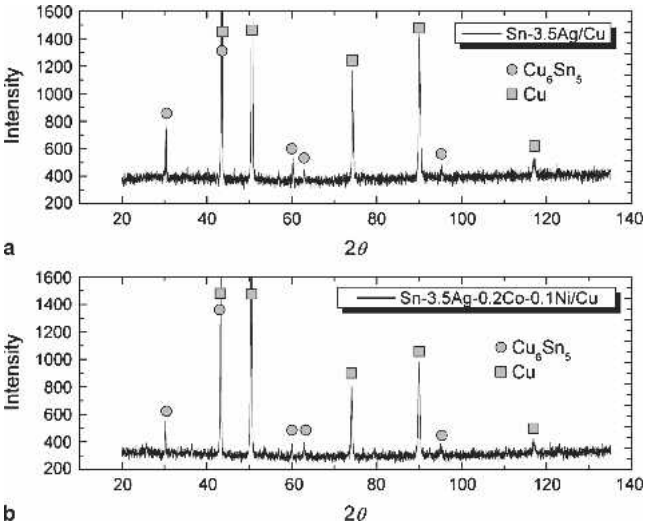

Fig. 5. XRD pattern of IMCs: (a) Sn-3.5Ag/Cu and (b) Sn-3.5Ag-0.2Co-0.1Ni/Cu.

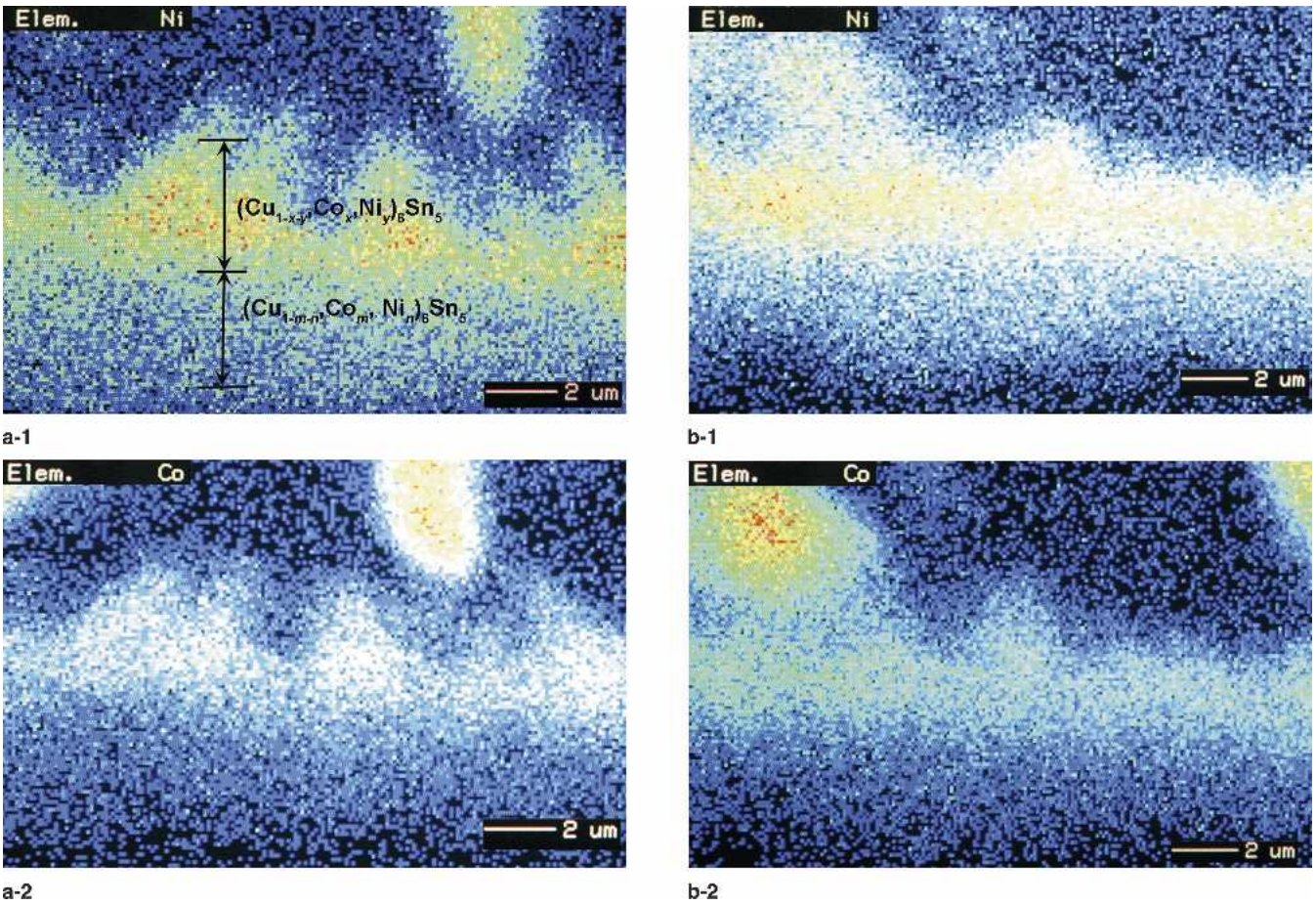

Fig. 6. Color-map analysis depicting the two distinct intermetallic regions $(Cu_{(1-x-y)}, Ni_x, Co_y)_6Sn_5 + (Cu_{(1-m-n)}, Ni_m, Co_n)_6Sn_5$: (a) as reflowed,

intermetallic region adjacent to the solder matrix, site 3 was close to the interface of intermetallic/Cu to probe the Cu_3Sn phase, and site 2 was defined in the middle. Table I depicted the tested results, and the plausible phases were also listed based on the concentration ratio and the XRD pattern results from Fig. 5, which indicted that the IMC was Cu_6Sn_5 based. The strong peak of Cu in Fig. 5 was from the Cu substrate. The additive couples Ni-Co were detected at the $(Cu, Ni, Co)_6Sn_5$ IMC region. However, they were not probed in the Cu_3Sn phase, which indicated that Ni and Co did not participate in the formation of Cu_3Sn phase. The nonuniform concentration distributions of additives Co-Ni were revealed within the entire $(Cu, Ni, Co)_6Sn_5$ intermetallic region, and the duplex structure phases for the $(Cu, Ni, Co)_6Sn_5$ intermetallic region could be suggested as $(Cu_{(1-x-y)}, Co_x, Ni_y)_6Sn_5 + (Cu_{(1-m-n)}, Co_m, Ni_n)_6Sn_5$. Here, the former represented the upper intermetallic phase with higher values of x and y than m and n for the latter, namely, the inner intermetallic phase that is adjacent to the Cu_3Sn phase (after aging treatment) or Cu substrate (no aging treatment).

In order to identify the duplex microstructure of the $(Cu, Ni, Co)_6Sn_5$ intermetallic region, the mapping analysis was performed using EPMA, as illustrated in Fig. 6. Apparently the concentration distribution of Ni-Co was not uniform, that is, the upper intermetallic adjacent to the solder matrix contained much higher Ni and Co concentration. After aging at 110°C, 130°C, and 150°C, respectively, the duplex structure was still present. However, the Ni and Co concentrations decreased with the aging temperature, especially at 130°C and 150°C, as shown in Fig. 7.

THERMODYNAMIC MODEL FOR THE MULTICOMPONENT ALLOY

In order to analyze the influence of additives during the interfacial reaction, the thermodynamic models were employed herein. Actually, for the i-j-k-m quaternary alloy system, the excess Gibbs energy ΔG^E could be assessed by the following formulation:[10]

$$\Delta G^E = \frac{x_i x_j}{X_{i(ij)} \cdot X_{j(ij)}} \cdot \Delta G_{ij} + \frac{x_i x_k}{X_{i(ik)} \cdot X_{k(ik)}} \cdot \Delta G_{ik} + \frac{x_i x_m}{X_{i(im)} \cdot X_{m(im)}} \cdot \Delta G_{im} + \frac{x_j x_k}{X_{j(jk)} \cdot X_{k(jk)}} \cdot \Delta G_{jk} + \frac{x_j x_m}{X_{j(jm)} \cdot X_{m(jm)}} \cdot \Delta G_{jm} + \frac{x_k x_m}{X_{k(km)} \cdot X_{m(km)}} \cdot \Delta G_{km} \quad (1)$$

where x_a (a = i, j, k, and m) denotes the component element concentration in the quaternary alloy system, and $X_{i(ij)}$, $X_{i(ik)}$, $X_{i(im)}$, $X_{j(jk)}$, $X_{j(jm)}$, and $X_{k(km)}$ represent the modified component element

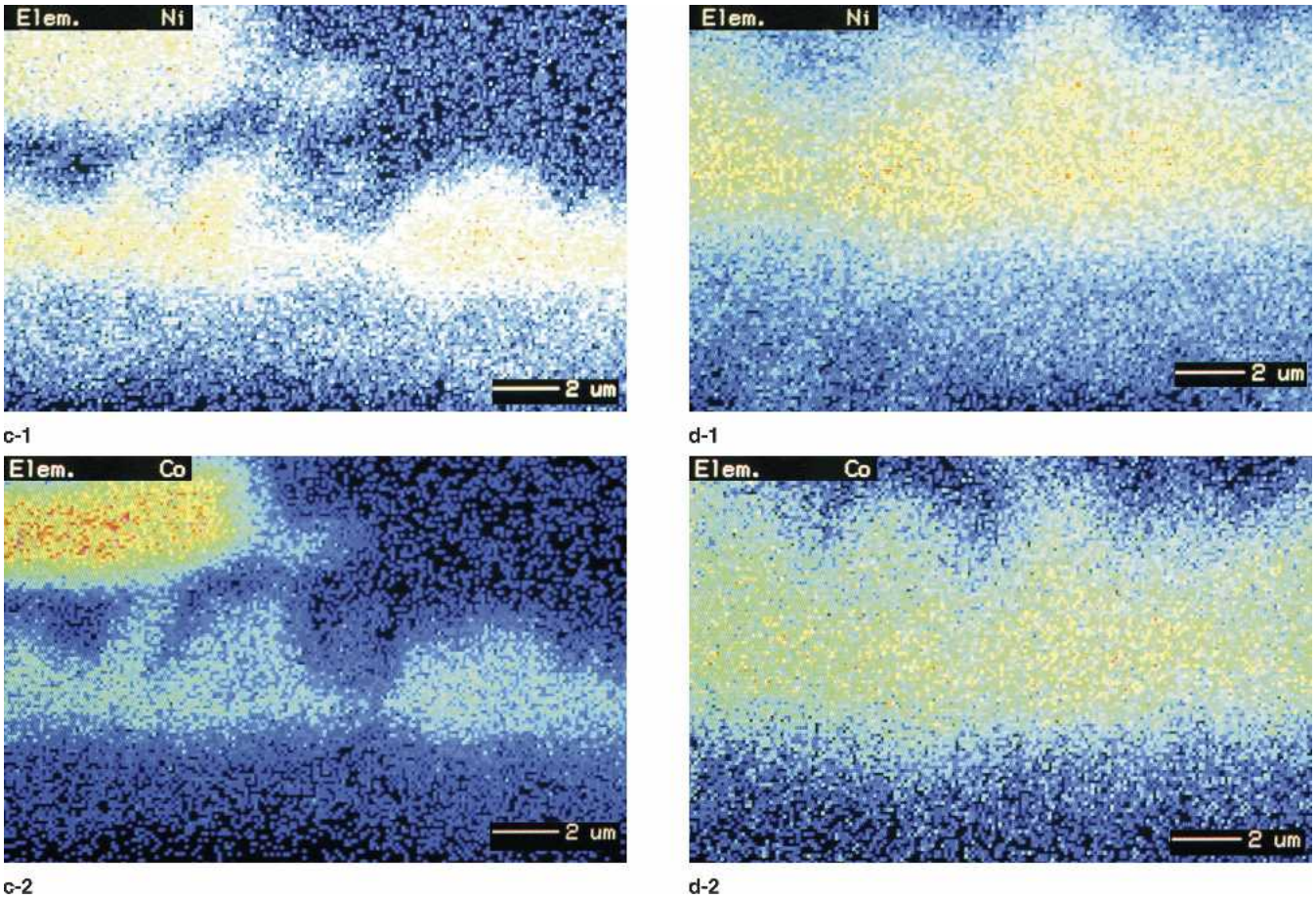

(b) aged at 110°C for 504 h, (c) aged at 130°C for 504 h, and (d) aged at 150°C for 504 h.

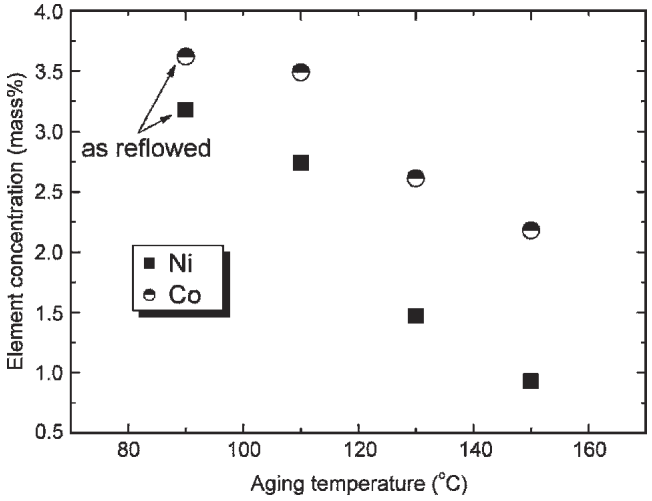

Fig. 7. Ni and Co concentration evolution at the outer IMC region with the aging temperature, namely, 110°C, 130°C, and 150°C, respectively.

concentrations in the corresponding binary alloy systems by introducing the similarity coefficient $\xi_{i(ij)}^{\langle k\rangle}$, which is defined as follows:[10]

$$X_{i(ij)} = x_i + \sum_{\substack{k=1 \\ k\neq i,j}}^{n} x_k \cdot \xi_{i(ij)}^{\langle k\rangle} \tag{2}$$

$$\text{where } \xi_{i(ij)}^{\langle k\rangle} = \frac{\eta(ij,ik)}{\eta(ij,ik)+\eta(ji,jk)} \tag{3}$$

where the deviation sum of squares yields

$$\eta(ij,ik) = \int_{X_i=0}^{X_i=1} (\Delta G_{ij}^{E} - \Delta G_{ik}^{E})^2 dX_i \tag{4}$$

Thus, if the component element k or m is considered as solvent, and the other three elements as solute, the interaction parameter ε_i^j can be calculated by

$$\varepsilon_i^j = \frac{1}{RT}\left(\frac{\partial^2 G^E}{\partial x_i \partial x_j}\right) \tag{5}$$

Actually, at the initial stage of soldering, the Cu atoms dissolve into liquid solder, and the saturation solution is generated at the interface between the solder matrix and the Cu substrate. Since the element Ag does not participate in the interfacial reaction, this local region solution system can be simplified as the Sn-Cu-Ni-Co quarternary alloy system. Consequently, the interaction parameters ε_{Sn}^{Ni}, ε_{Sn}^{Co}, and ε_{Sn}^{Cu}, are predicted to evaluate the affinity among these component elements, as shown in Fig. 8.

All the values of ε_{Sn}^{Ni}, ε_{Sn}^{Co}, and ε_{Sn}^{Cu} are negative, which indicates that Sn-Cu, Sn-Ni, and Sn-Co are all possible to form intermetallics. However, the absolute values of ε_{Sn}^{Ni} and ε_{Sn}^{Co} are larger than ε_{Sn}^{Cu}, which means that the affinities of Sn-Ni and Sn-Co are higher than that of the Sn-Cu couple. That can explain qualitatively why both Ni and Co are involved in the formation of the intermetallic. The higher concentration of Ni and Co in the upper intermetallic region may be attributed to enhancing the driving force of IMC formation and reducing the interfacial energy between the IMC and the solder matrix during the soldering process, which will be addressed elsewhere.

MECHANICAL RESPONSE OF NONHOMOGENOUS (Cu, Co, Ni)$_6$Sn$_5$ INTERMETALLIC

Based on the previous observation and measurement, it has been confirmed that the additive Ni-Co at the entire (Cu, Co, Ni)$_6$Sn$_5$ intermetallic region is not distributed evenly. Therefore, it is expected that the mechanical properties for this portion of the intermetallic region are also nonhomogeneous.

Since the mechanical properties of the intermetallic could significantly impact the reliability of solder joint, it would be very essential to estimate some of the primary mechanical properties, such as hardness, Young's modulus, etc. The widely concerned nanoindentation technology was adopted in this study. The accuracy of the indentation equipment (Micro Materials, Wrexham, United Kingdom) assembled with the Berkovich indenter could ensure the reliable data for the small load (e.g., 2 mN) on the defined positions. The testing positions, namely site 1 and site 2, were selected, as shown in Fig. 3, while the Cu$_3$Sn phase was not included here due to its quite small size.

It has been known that the reduced Young's modulus could be obtained from measuring the contact stiffness at the onset of the unloading segment.[11]

$$E_r = \frac{\sqrt{\pi}}{2\beta}\cdot\frac{S}{\sqrt{A}} \tag{6}$$

where S is the contact stiffness, β is a constant related to the geometry of the indenter, and A is the projected area by indentation. Meanwhile, the reduced Young's modulus could be given by

$$E_r = \left[\frac{1-\nu^2}{E} + \frac{1-\nu_{in}^2}{E_{in}}\right]^{-1} \tag{7}$$

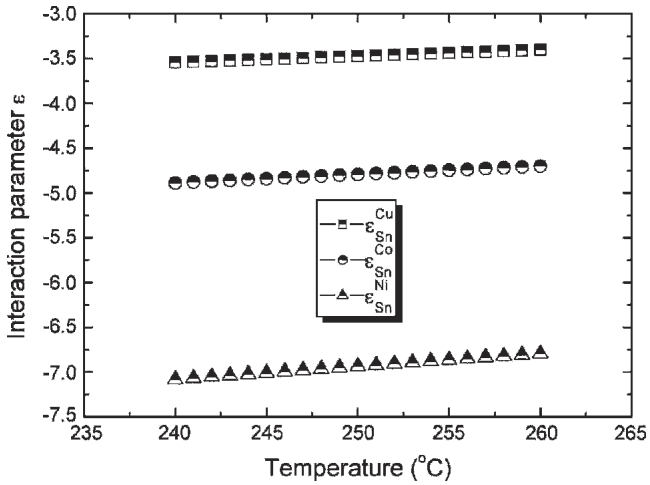

Fig. 8. The predicted affinity of Sn-Cu, Sn-Ni, and Sn-Co, respectively, in the Sn-Cu-Co-Ni quarternary system.

Table II. Nonhomogeneous Mechanical Properties of (Cu, Co, Ni)$_6$Sn$_5$ by Nanoindentation

Condition	Phases	Sites	Hardness H (GPa)	Young's Modulus E (GPa)
As reflowed	$(Cu_{(1-x-y)}, Co_x, Ni_y)_6Sn_5$	1	2.12 ± 0.54	86.6 ± 6.5
	$(Cu_{(1-m-n)}, Co_m, Ni_n)_6Sn_5$	2	3.81 ± 0.43	97.8 ± 7.1
Aging at 150°C	$(Cu_{(1-x-y)}, Co_x, Ni_y)_6Sn_5$	1	4.15 ± 0.14	103.5 ± 6.7
	$(Cu_{(1-m-n)}, Co_m, Ni_n)_6Sn_5$	2	5.04 ± 0.22	114.3 ± 3.2

where E and ν denote the Young's modulus and Poisson's ratio of the indented material, respectively, while E_{in} and ν_{in} represent the parameters to the indenter, which can be taken as 1,140 GPa and 0.07, respectively.[12] In addition, the hardness H is represented by the maximum force P_{max} divided by the projected indentation area A, which could be derived from the Oliver–Pharr method.[11]

$$H = \frac{P_{max}}{A} \tag{8}$$

Table II depicted the hardness and Young's modulus of (Cu, Co, Ni)$_6$Sn$_5$ intermetallic at differing positions, namely, outer and inner regions. Apparently, the nonhomogenous mechanical properties of (Cu, Co, Ni)$_6$Sn$_5$ intermetallic were revealed. The upper intermetallic region $(Cu_{(1-x-y)}, Co_x, Ni_y)_6Sn_5$ bearing higher additives (i.e., Ni and Co) possesses a more greatly reduced hardness and Young's modulus than that for the inner region $(Cu_{(1-m-n)}, Co_m, Ni_n)_6Sn_5$. It can be reasoned that the participation of additives in the Cu_6Sn_5 crystal microstructure cause the disordered crystal lattices or some defects. In addition, the solder entrapped within the (Cu, Co, Ni)$_6$Sn$_5$ IMC will also be partly responsible for this result due to the quite low values of these parameters. The results displayed in Table II indicated that the involvement of additives (i.e., Ni and Co) in the (Cu, Co, Ni)$_6$Sn$_5$ region, as well as the loose morphology owing to the entrapped solder inside, could improve the ductile property of IMCs, while after the aging process, the hardness and the modulus increased for both inner and outer intermetallic regions. The reason could be that the solder entrapped within the intermetallic tended to be converted into intermetallics, as well as the morphology modification during the solid aging process.

CONCLUSIONS

The following conclusions can be summarized.

- The morphology of IMCs formed between Sn-3.5Ag-0.2Co-0.1Ni solder and Cu was converted into columnar like, which was quite different from the typical scallop like for Sn-Ag/Cu. The reduced growth rate of IMC during the early aging time or lower aging temperature was attributed to the nondense intermetallic morphology with some solder entrapped in the intermetallic region. After the solid aging process, the Cu_3Sn phase was not generated at 110°C for 504 h, while it appeared at 130°C at some selected sites. A continuous Cu_3Sn layer was observed at 150°C.
- After reflow, the chemical composition of intermetallic between Sn-Ag-Co-Ni solder and Cu was identified as (Cu, Ni, Co)$_6$Sn$_5$. Two distinct IMC regions, namely, the outer region adjacent to the solder matrix and the inner region neighboring to the Cu substrate, were detected. The outer IMC region contained much higher Co and Ni concentrations than those at the inner region. After aging, this duplex structure was still present, while another phase, namely, Cu_3Sn was generated.
- The mechanical properties of (Cu, Ni, Co)$_6$Sn$_5$ intermetallic were estimated by nanoindentation. The hardness and Young's modulus of the upper (Cu, Ni, Co)$_6$Sn$_5$ intermetallic, which bear higher additives, were all lower than those for the inner intermetallic region. After aging, the hardness and modulus of the intermetallic were all elevated, which could be attributed to the consumption of solder entrapped within the intermetallic, as well as the intermetallic morphology change.

ACKNOWLEDGEMENTS

The financial support from the Japan Society for the Promotion of Science (JSPS) is greatly acknowledged. This research work had been presented at the 2005 TMS Meeting & Exhibition symposium on "Phase Stability, Phase Transformation and Reactive Phase Formation in Electronic Materials IV" (San Francisco, CA, Feb. 13–17, 2005).

REFERENCES

1. T. Laurila, V. Vuorinen, and J.K. Kivilahti, *Mater. Sci. Eng. R* 49, 1 (2005).
2. K. Zeng and K.N. Tu, *Mater. Sci. Eng. R* 38, 55 (2002).
3. F. Guo, J. Lee, S. Choi, J.P. Lucas, T.R. Bieler, and K.N. Subramanian, *J. Electron. Mater.* 30, 1073 (2001).
4. C.-M. Chuang and K.-L. Lin, *J. Electron. Mater.* 32, 1426 (2003).
5. K.S. Kim, S.H. Huh, and K. Suganuma, *Microelectron. Reliab.* 43, 259 (2003).
6. I.E. Anderson, J.C. Foley, B.A. Cook, J. Harringa, R.L. Terpstra, and O. Unal, *J. Electron. Mater.* 30, 1050 (2001).
7. J.Y. Tsai, Y.C. Hu, C.M. Tsai, and C.R. Kao, *J. Electron. Mater.* 32, 1203 (2003).
8. A.M. Gusak and K.N. Tu, *Phys. Rev. B: Condens. Matter Mater. Phys.* 66, 115403-1 (2002).
9. H.K. Kim and K.N. Tu, *Phys. Rev. B: Condens. Matter Mater. Phys.* 53, 16027 (1996).
10. K.C. Chou and S.K. Wei, *Metall. Mater. Trans. B* 28, 439 (1997).
11. W.C. Oliver and G.M. Pharr, *J. Mater. Res.* 7, 1564 (1992).
12. J.A. Knapp, D.M. Fllstaedt, S.M. Myers, J.C. Barbour, and T.A. Friedmann, *J. Appl. Phys.* 85, 1460 (1999).